Empty-Level Structure and Reactive Species Produced by Dissociative Electron Attachment to tert-Butyl Peroxybenzoate

ARTICLE *in* THE JOURNAL OF PHYSICAL CHEMISTRY A · MARCH 2012

Impact Factor: 2.69 · DOI: 10.1021/jp300643e · Source: PubMed

THE JOURNAL OF PHYSICAL CHEMISTRY A

Article

pubs.acs.org/JPCA

Empty-Level Structure and Reactive Species Produced by Dissociative Electron Attachment to *tert*-Butyl Peroxybenzoate

Alberto Modelli*,† and Stanislav A. Pshenichnyuk‡

†Dipartimento di Chimica "G. Ciamician", Università di Bologna, via Selmi 2, 40126 Bologna, Italy, and Centro Interdipartimentale di Ricerca in Scienze Ambientali, via S. Alberto 163, 48123 Ravenna, Italy

‡Institute of Physics of Molecules and Crystals, Ufa Research Center of RAS, October Prospect, 151, Ufa 450075, Russia

ABSTRACT: The energy and nature of the gas-phase temporary anion states of *tert*-butylperoxybenzoate in the 0−6 eV energy range are determined for the first time by means of electron transmission spectroscopy (ETS) and appropriate theoretical calculations. The first anion state, associated with electron capture into a delocalized π^* MO with mainly ring and carbonyl character, is found to lie close to zero energy, i.e., sizably more stable (about 2 eV) than the ground (σ^*) anion state of saturated peroxides. Dissociative decay channels of the unstable parent molecular anions are detected with dissociative attachment spectroscopy (DEAS), as a function of the incident electron energy, in the 0−14 eV energy range. A large DEA cross-section, with maxima at zero energy, 0.7 and 1.3 eV, is found for production of the (m/e = 121) $PhCOO^-$ anion fragment, together with the corresponding *tert*-butoxy neutral radical, following cleavage of the O−O bond. Although with much smaller intensities, a variety of other negative currents are observed and assigned to the corresponding anion fragments with the support of density functional theory calculations.

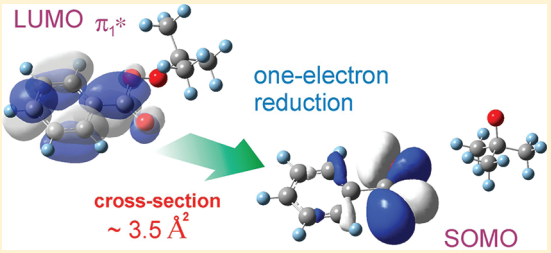

1. INTRODUCTION

The reactivity of the organic peroxides RO−OR′, where the R and R′ groups can be either saturated or unsaturated hydrocarbons, is closely associated with the weakness of the O−O bond that can be broken easily following several mechanisms,[1] the bond dissociation energy generally ranging from 20 to 50 kcal mol^{-1}. Thermal and photoinduced decomposition of organic peroxides have been investigated[2−5] in considerable detail. This class of compounds represents a strong free-radical source, so that peroxides are extensively used as initiators in free-radical polymerizations[5−7] (an efficient synthetic method in modern polymer chemistry), as curing agents in the petrochemical industry, and as active components of cosmetics and pharmaceuticals.[8] Unfortunately, the use of organic peroxides is associated with hazards such as explosion, fire, and toxicity. In particular, organic peroxides react violently with reducing agents.[9]

Highly reactive oxygen species, which include the superoxide anion, hydrogen peroxide, and the hydroxyl free radical, are produced in vivo by the mitochondrial electron transport chain.[10,11] Large concentrations of these species lead to human diseases such as atherosclerosis, Parkinson's disease, heart failure, Alzheimer's disease, and cancer.[12−15] Owing to the involvement of free radicals in carcinogenic processes,[16−19] the ability of organic peroxides to stimulate radical production in mitochondria is found to be strongly correlated with their tumor-promoting activity.[20−22] A review that summarizes many studies of the carcinogenicity of organic peroxides using rodent models has been reported by Kraus et al.[23] More recently, organic peroxides, including *tert*-butyl peroxybenzoate (**TBPB**), have been identified as tumor promoters in mouse skin.[24]

Xenobiotic molecules can in principle penetrate through the outer mitochondrial membrane and interact with electrons. Under reductive conditions, peroxides produce neutral radicals and anion species through the mechanism referred to as dissociative electron transfer,[25−27] promoted by the electron carrying component (cytochrome *c*) of the mitochondrial electron transport chain.[28] Studies of electrochemical reduction of organic peroxides in solution were reported by Maran and co-workers[29−31] and Baron et al.[32]

In some cases, when the toxicity is directed against parasites, the xenobiotic activity of radical species produces beneficial effects. This is the case for artemisinin (a polycyclic molecular system containing an endoperoxidic bond), an antimalarial drug effective against multidrug-resistant malarial parasite strains such as *Plasmodium falciparum*.[33] In addition, this molecular system seems also to present antitumor activity.[34]

While electrode reduction reactions in solution do not allow an easy characterization of the radicals produced, electron attachment reactions in the gas phase are more suitable for detailed experimental investigations, using two complementary techniques. Electron transmission spectroscopy (ETS)[35,36] measures the energies of vertical electron attachment into empty molecular orbitals (MOs) to form temporary molecular anion states, a process also referred to as shape resonance.

Received: January 19, 2012
Revised: March 19, 2012
Published: March 19, 2012

Dissociative electron attachment spectroscopy (DEAS)[36,37] reveals the presence of dissociative decay channels of these molecular anions formed by resonance and measures the yields of the various negative fragments produced, as a function of the incident electron energy. In fact, when suitable energetic conditions occur, the decay of unstable molecular anions can follow a dissociative channel, which generates negative fragments (usually sufficiently long-lived to be detected with a mass filter) and neutral radicals

$$e^-_{(E)} + AX \rightarrow AX^- \rightarrow A + X^-$$

in kinetic competition with simple re-emission of the extra electron.

After having applied these techniques to artemisinin and the simpler reference molecule di-*tert*-butylperoxide (**DTB**)[38,39] (where only single bonds are present except for a carbonyl functional group in the former), in this study, the ETS and DEAS techniques, with the support of density functional (DFT) calculations, are used to elucidate the empty-level structure of **TBPB** (represented in Scheme 1), which possesses

Scheme 1. *tert*-Butyl Peroxybenzoate (TBPB)

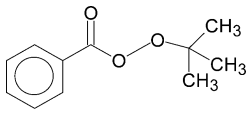

a large conjugated π-system adjacent to the peroxidic bond, characterize the neutral and negative reactive fragment species produced by dissociative decay channels of the parent molecular anions, and evaluate their relative intensities.

2. EXPERIMENTAL METHODS

Our electron transmission apparatus (Bologna Laboratory) is in the format devised by Sanche and Schulz[35] and has been previously described.[40] To enhance the visibility of the sharp resonance structures, the impact energy of the electron beam is modulated with a small ac voltage, and the derivative of the electron current transmitted through the gas sample is measured directly by a synchronous lock-in amplifier. Each resonance is characterized by a minimum and a maximum in the derivative signal. The energy of the midpoint between these features is assigned as the vertical attachment energy (VAE). The spectrum of **TBPB** was obtained using the apparatus in the high-rejection mode[41] and is, therefore, related to the nearly total scattering cross-section. The electron beam resolution was about 50 meV full width at half-maximum (fwhm). The energy scale was calibrated with reference to the $(1s^12s^2)\ ^2S$ anion state of He. The estimated accuracy is ±0.05 or ±0.1 eV, depending on the number of decimal digits reported.

The collision chamber of the ETS apparatus has been modified[42] to allow for ion extraction at 90° with respect to the incident electron beam direction. Ions are then accelerated and focused toward the entrance of a quadrupole mass filter. Alternatively, the total anion current can be collected and measured with a picoammeter at the walls of the collision chamber (about 0.8 cm from the electron beam). Measurements of the total and mass-selected anion currents were obtained with an incident electron beam current about twice as large as that used for the ET experiment. The energy spread of the electron beam increased to about 110 meV (fwhm), as evaluated from the width of the SF_6^- signal at zero energy used for calibration of the energy scales.

In order to observe the most weak signals, although with a smaller energy resolution of the incident electron beam, a negative ion magnetic mass spectrometer (Ufa Laboratory), described in detail previously,[43,44] has been used. Briefly, an electron beam of defined energy is passed through a collision cell containing a vapor of the substance under investigation, under single-collision conditions. A current of magnetically mass-selected negative ions is recorded as a function of the incident electron energy in the 0−14 eV energy range. The electron energy scale is calibrated with the zero energy SF_6^- signal. The fwhm of the electron energy distribution is 0.4 eV, and the accuracy of the measured peak positions is estimated to be ±0.1 eV.

The **TBPB** sample was commercially available (Aldrich #159042) and used without further purification. The collision cell of both instrumentations was kept at about 80 °C, thus preventing thermal decomposition.[45]

Calculations were carried out with the Gaussian09 set of programs.[46] Evaluation of the virtual orbital energies (VOEs) of the neutral molecule was performed at the B3LYP/6-31G(d) level of theory.[47] The vertical electron affinity (EA_v) was calculated as the difference between the total energy (only electronic contributions) of the neutral and the lowest anion state, both in the optimized geometry of the neutral state, using the B3LYP hybrid functional with the standard 6-31+G(d) basis set, which includes the minimum addition of diffuse functions. The adiabatic electron affinity (EA_a) was obtained as the energy difference between the neutral and the lowest anion state, each in its optimized geometry.

3. RESULTS AND DISCUSSION

3.1. Geometry and Dissociation Energy of the Neutral Molecule. The geometry of neutral **TBPB** optimized with B3LYP/6-31+G(d) calculations is represented in Figure 1. As

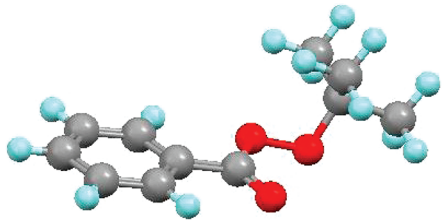

Figure 1. Representation of the geometry of **TBPB** in its ground neutral state, as optimized with B3LYP/6-31+G(d) calculations.

expected, the conjugated ring-carbonyl π-system is nearly coplanar, and also, the O−O bond lies nearly in the same plane of the C═O double bond, forming with it an OCOO dihedral angle of 7.5° (quite close to that obtained with the 6-31G(d) basis set or the MP2/6-31G(d) method). The B3LYP/6-31+G(d) O−O bond length of **TBPB** is predicted to be 1.451 Å, which is somewhat shorter than that calculated for the saturated peroxides RO−OR, with R = *tert*-butyl (1.475 Å), methyl (1.471 Å), and H (1.467 Å). The latter is in good agreement with a microwave gas-phase determination of 1.463 Å.[48]

The thermodynamic energy threshold for homolytic cleavage of the O−O bond, calculated as the total energy (only electronic contributions) difference between the two radical fragments and the undissociated neutral molecule, is 1.209 eV

dx.doi.org/10.1021/jp300643e | J. Phys. Chem. A 2012, 116, 3585−3592

(27.9 kcal mol^{-1}) for **TBPB** and 1.325 eV (30.6 kcal mol^{-1}) for **DTB** at the B3YP/6-31+G(d) level. The corresponding values obtained with the 6-31G(d) basis set, 1.372 eV (31.6 kcal mol^{-1}) for **TBPB** and 1.526 eV (35.2 kcal mol^{-1}) for **DTB**, are somewhat larger. The latter is in fairly good agreement with bond dissociation enthalpy values (which range from 38.0 to 42.9 kcal mol^{-1}[49−52]) measured in **DTB**. In any case, according to both basis sets, the bond dissociation energy of **TBPB** is smaller (about 90%) than that of di-*tert*-butyl peroxide, thus favoring the O−O bond cleavage with other conditions being the same.

3.2. Electron Attachment Energies. An isolated molecule can temporarily attach an electron of proper energy and angular momentum into a vacant MO, a process being referred to as a shape resonance.[36] ETS[35] is one of the most suitable means for detecting the formation of unstable anions. Because electron attachment is rapid with respect to nuclear motion, temporary anions are formed with the equilibrium geometry of the neutral molecule. The impact electron energies at which electron attachment occurs are properly denoted as vertical attachment energies (VAEs) and are the negative of the vertical electron affinities. Within the Koopmans' theorem approximation,[53] VAEs are equal to the corresponding empty MO energies.

A theoretical approach adequate for describing the nature and energy of unstable anion states involves difficulties not encountered for neutral or cation states.[54−57] EAs can be obtained as the difference between the total energies of the neutral and anion ground states, both at the optimized geometry of the neutral species (EA_v) or each with its optimized geometry (EA_a). A proper description of the spatially diffuse electron distributions of anions normally requires a basis set with diffuse functions.[58,59] However, calculated anion state energies decrease as the basis set is expanded, so that the choice of a basis set that gives a satisfactory description of the energy and nature of the anion is a priori not obvious.[60] In general, the more unstable the anion state, the greater the need to augment the basis set with diffuse functions, increasing the risk that the singly occupied MO (SOMO) of the anion is described as a diffuse function with no physical significance with respect to anion formation.[54,55,60,61]

However, analyses of the use of Koopmans' theorem calculations for the evaluation of VAEs demonstrated the occurrence of good linear correlations between the π^* VAEs measured in a large number of alkenes and benzenoid hydrocarbons and the corresponding virtual orbital energies (VOEs) of the neutral molecules obtained with Hartree−Fock[54,56] or B3LYP[61] calculations, using basis sets without diffuse functions. A more accurate correlation is expected if the scaling equation is calibrated with training compounds structurally close to the subject molecule. This approach also provided similar correlations for the σ^* VAEs of a series of group 14 mixed dimers,[62] chloroalkanes,[63] and bromoalkanes[64] (although it was shown that these empirical correlations are strongly dependent on the molecular structures and the nature of the σ^* MOs). In addition, anion states associated with σ^* MOs generally lie at higher energy and have a shorter lifetime than those associated with π^* MOs, hence giving rise to broader shape resonances. Narrow low-energy σ^* resonances were in fact observed only in compounds containing third-row or heavier elements.[65]

Figure 2 displays the ET spectrum of **TBPB**, where the vertical lines locate the most probable VAEs (0.82, 2.67, and 4.5 eV) of three pronounced resonances. Table 1 reports the

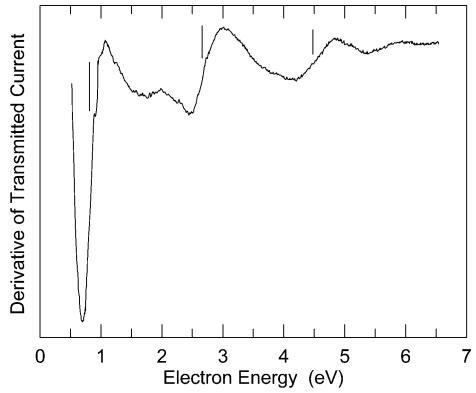

Figure 2. Derivative of transmitted current, as a function of electron energy, in gas-phase **TBPB**. Vertical lines locate the π_2^*−π_4^* VAEs.

Table 1. B3LYP/6-31G(d) Virtual Orbital Energies of TBPB, Scaled Values (See Text) and Measured VAEs[a]

orbital	VOE	scaled[b]	VAE
$\pi_4^*{}_{ring/CO}$	4.563	4.60	4.5
$\pi_3^*{}_{CO/ring}$	1.545	2.17	2.67
$\sigma^*{}_{O-O}$	0.315	1.87[c]	∼2.0
$\pi_2^*{}_{ring}$	−0.268	0.70	0.82
$\pi_1^*{}_{ring/CO}$	−1.284	−0.12	

[a]All values in electronvolts. [b]π^* scaling from ref 66. [c]σ^* scaling from ref 63.

B3LYP/6-31G(d) VOEs of the four π^* empty MOs and the first σ^* empty MO (with mainly O−O antibonding character) of **TBPB**, and the corresponding scaled VOEs and, for the sake of comparison, the VAEs measured in the ET spectrum. The π^* VOEs were scaled with an empirical linear correlation ($VAE_{(eV)}$ = 0.8065 × VOE + 0.9194) found for π^* MOs of alternating phenyl and ethynyl groups,[66] while the $\sigma^*{}_{O-O}$ VOE, in the absence of more appropriate correlations, was scaled with a linear equation ($VAE_{(eV)}$ = 0.8111 × VOE + 1.6097) found for the $\sigma^*{}_{C-Cl}$ MOs of chloroalkanes.[63]

The scaling procedure leads to predict the first vertical anion state to be slightly (0.12 eV, see Table 1) more stable than the neutral molecule (a negative VAE corresponds to a positive EA_v), indicating that formation of the π_1^* anion cannot be detected with ETS. This result is in nice agreement with an independent evaluation of EA_v, obtained as the B3LYP/6-31+G(d) total energy difference between the vertical anion and the neutral states. Once the correction for zero-point vibrational energies is accounted for (see Table 2), the first vertical anion state results to be 0.09 eV more stable than the neutral state. Also, it should be noted that both the LUMO of the neutral molecule and the SOMO of the vertical anion are correctly described as valence π^* orbitals.

The three intense resonances observed in the ET spectrum of **TBPB** in the 0−5 eV energy range are thus associated with the π_2^*−π_4^* anion states, their VAEs being reproduced by the scaled VOEs within ±0.1 eV, except for π_3^*. The weaker but distinct and relatively narrow signal located at about 5.6 eV is thus plausibly ascribed to a core-excited resonance (electron capture accompanied by excitation of a valence electron), in line with a corresponding feature observed in the same energy range in benzaldehyde.[67]

The ET spectrum of the saturated **DTB** molecule[38] displays a resonance centered at 2.0 eV, associated with electron capture

dx.doi.org/10.1021/jp300643e | J. Phys. Chem. A 2012, 116, 3585−3592

Table 2. B3LYP/6-31+G(d) Energies (eV) Relative to the Neutral Ground State of TBPB[a]

m/e		energy (eV)
194	vertical anion	0.066 (−0.089)
194	adiabatic anion[b]	−2.504 (−2.647)
121	$PhCOO^- + t\text{-}BuO^\bullet$	−2.224 (−2.387)
89	$PhCO^\bullet + (CH_3)_2(OCH_3)CO^-$	−0.529 (−0.752)
89	$PhCO^\bullet + t\text{-}BuOO^-$	1.947 (1.732)
89	$Ph^\bullet + CO + t\text{-}BuOO^-$	3.242 (2.886)
89	$PhC^- + t\text{-}BuO^\bullet + O_2$	7.118 (6.695)
89	$PhC^- + t\text{-}BuOOO^\bullet$	7.340 (7.020)
85	$PhO^\bullet + CH_4 + CH_2{=}C(CH_3)COO^-$ (1)	−2.074 (−2.406)
85	$PhO^\bullet + CH_4 + CH(CH_3){=}C(H)COO^-$ (2)	−2.014 (−2.341)
85	$PhO^\bullet + CH_4 + CH(CH_3){=}C(H)COO^-$ (3)	−1.981 (−2.322)
85	$PhO^\bullet + CH_4 +$ *cyc.* $CH_2CH_2OC(O)CH^-$ (4)	−1.055 (−1.346)
85	$PhOO^\bullet + t\text{-}BuCO^-$	2.866 (2.600)
77	$Ph^- + CO_2 + t\text{-}BuO^\bullet$	0.458 (0.159)
77	$Ph^- + t\text{-}BuOOCO^\bullet$	3.396 (3.146)
73	$PhCOO^\bullet + t\text{-}BuO^-$	−0.514 (−0.737)
73	$Ph^\bullet + CO_2 + t\text{-}BuO^-$	−0.326 (−0.627)
58	$PhCOOCH_3 + (CH_3)_2CO^-$	−1.337 (−1.514)
57	$PhCOO^\bullet + CH_4 + C_3H_5O^-$	−0.726 (−0.883)
57	$PhO^\bullet + CO_2 + t\text{-}Bu^-$	0.091 (−0.268)
57	$PhCOOO^\bullet + t\text{-}Bu^-$	3.416 (3.127)
44	Ph-O-*t*-Bu + CO_2^-	−1.587 (−1.739)
15	$PhCOO^\bullet + (CH_3)_2CO + CH_3^-$	1.552 (1.109)

[a]The values in parentheses include zero-point vibrational energy corrections. [b]See text and Figure 4.

into the σ^*_{O-O} lowest unoccupied MO (LUMO). This signal is relatively broad and weak, in line with the small cross-section of σ^* resonances in molecules with light elements.[65] Similar σ^*_{O-O} VAEs (1.7−1.8 eV) were found in the polycyclic peroxides artemisinin and arthemeter.[38] Indeed, the ET spectrum of **TBPB** displays a feature around 2.0 eV (see Figure 2), partially superimposed upon the low-energy side of the higher-lying (and much more intense) π_3^* resonance. In agreement, the σ^*_{O-O} B3LYP/6-31G(d) VOE (see Table 1) is intermediate between the π_2^* and π_3^* VOEs, and although the scaling equation employed was calibrated with σ^*_{C-Cl} VAEs,[63] the scaled σ^*_{O-O} VOE leads to a VAE of 1.87 eV. We thus locate the σ^*_{O-O} resonance of **TBPB** at about 2.0 eV. The first three empty MOs, as obtained with B3LYP/6-31G(d) calculations, are represented in Figure 3. It is to be noted that, whereas, in **DTB**, the lowest anion state (σ^*_{O-O}) is sizably unstable, the first vertical anion state of **TBPB** lies near zero energy and is of π^* nature, both factors increasing the cross-section for anion formation in the latter.

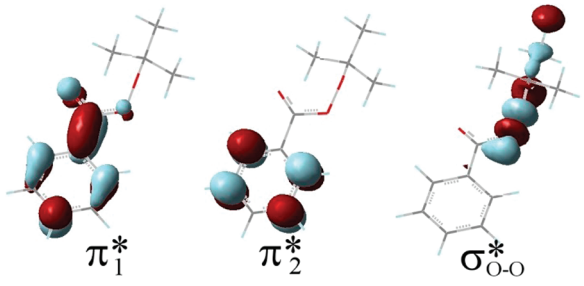

Figure 3. Representation of the three lowest-lying empty MOs of **TBPB**, as obtained with B3LYP/6-31G(d) calculations.

As reported in Table 2, the B3LYP/6-31+G(d) calculations find an energy minimum for the adiabatic anion state of **TBPB** much more stable (2.504 eV) than the neutral molecule, where the O−O distance is very large (4.58 Å, to be compared with the adiabatic anion of **DTB** where the O−O distance is only 2.387 Å). In fact, according to the calculations, this species is essentially dissociated and quite close to two separated fragments (see Figure 4). The calculated charge distributions

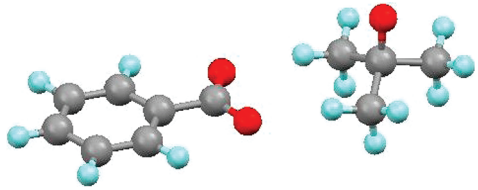

Figure 4. Representation of the geometrically relaxed anion state of **TBPB**, as obtained with B3LYP/6-31+G(d) calculations.

predict a negative charge of −0.936 *e* on the benzoate moiety and only −0.068 *e* on the *t*-butoxy group (labeled $PhCOO^-$ and $t\text{-}BuO^\bullet$, respectively, in Table 2).

3.3. DEA Spectra. Figure 5 reports the total anion current (measured at the walls of the collision cell) and by far the most

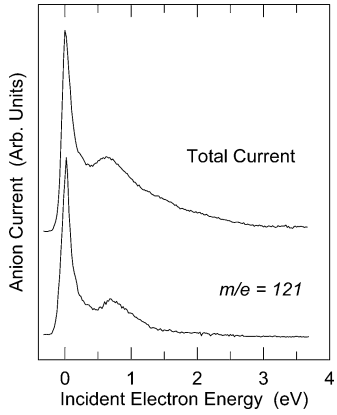

Figure 5. Total and fragment anion currents, as a function of incident electron energy, measured in **TBPB**.

intense mass-selected anion fragment (*m/e* = 121) obtained with an energy resolution of the incident electron beam of about 110 meV fwhm. Both display a sharp and intense peak at zero energy, followed by a distinct maximum at 0.7 eV and an unresolved shoulder at 1.3−1.4 eV. The total anion current is plausibly almost completely accounted for by the *m/e* = 121 negative fragment, generated by cleavage of the O−O bond of the parent molecular anion to give the $PhCOO^-$ anion and the neutral $t\text{-}BuO^\bullet$ radical. In agreement, the thermodynamic energy threshold calculated for the production of these fragments is largely negative (see Table 2).

The three observed DEA signals are ascribed to formation and dissociation of the first three anion states: the (vibrationally excited) π_1^* anion, the π_2^* anion, and the σ^*_{O-O} anion, the last two located at 0.82 eV and around 2.0 eV, respectively, in the ET spectrum. The shift of the DEA peaks to lower energy with respect to the corresponding VAEs measured in ETS is well understood in terms of shorter lifetime and greater distance to the crossing between the anion and neutral potential curves for the anions formed on the high-energy side of the resonance.[68]

dx.doi.org/10.1021/jp300643e | J. Phys. Chem. A 2012, 116, 3585−3592

This shift can be quite large (for instance, about 1 eV in 1-chloroalkanes[69]), depending on an inverse fashion upon the resonance lifetime, thus explaining the relatively small energy shift found for the π_2* resonance and the large shift of the σ^*_{O-O} resonance of **TBPB**. In fact, a shift quite similar to the latter was observed[39] in **DTP**, where the distinct σ* resonance of the ET spectrum is centered at 2.0 eV, and the corresponding m/e = 73 DEA current (associated with dissociation of the O−O bond and formation of the *t*-BuO$^-$ anion fragment) peaks at 1.3 eV, i.e., the same energy of the shoulder observed in the present DEA spectra of **TBPB**.

A quantitative evaluation of the total current measured in **TBPB** at zero energy (under defined conditions of sample pressure and intensity of the incident electron beam) leads to a DEA cross-section of 3.5×10^{-16} cm^2, i.e., about three times as large as that of bromobenzene at 0.66 eV.[70]

DEA spectra of **TBPB** were recorded in the 0−14 eV energy range using a more sensitive apparatus, with an electron beam energy spread of about 0.4 eV (fwhm). The results are displayed in Figure 6. In addition to the most intense m/e =

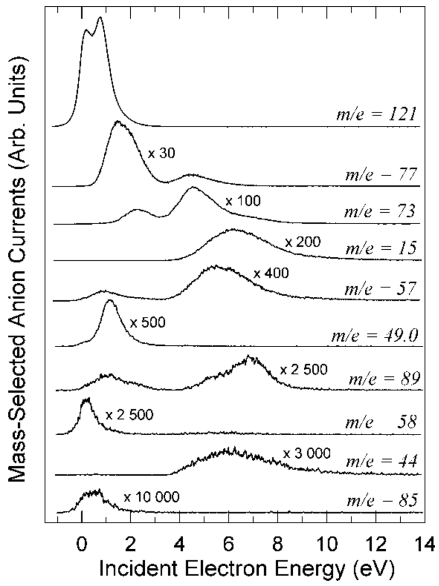

Figure 6. Mass-selected currents of negative ions formed by DEA to **TBPB** as a function of the incident electron energy.

121 anion current, at least nine more negative fragments were observed, with intensities 2 to 3 orders of magnitude smaller. Plausible structures of these anions, their energies of formation, and relative intensities are listed in Table 3. It can also be noted that under such instrumental conditions the relative heights of the zero and 0.7 eV m/e = 121 peaks are reversed (compare with Figure 5). This difference can be ascribed to convolution with the energy spread of the incident electrons, expected to lower the height of narrow signals, and possibly also to kinetic energy discrimination in the anion extraction efficiency of the mass spectrometer.

As a first comment, in spite of a relatively high EA$_a$ of **TBPB**, even the high-sensitivity DEA spectra do not reveal the presence of the undissociated parent molecular anion of **TBPB** (in the instrumental microsecond time scale).

Distinct maxima around 4.5 eV, like those observed in the m/e = 77 and m/e = 73 currents, are likely associated with formation of the fifth (π_4*) anion state, located at the same

Table 3. Most Probable Structures of Fragment Anions Formed by DEA to TBPB, Peak Energies (eV), and Relative Intensities (Evaluated from Peak Heights)

m/e	anion structure	peak energy	relative intensity
15	CH_3^-	6.2	0.1
44	CO_2^-	6.0	<0.1
49.0	m* 121 → 77[a]	1.2	0.1
57	$C_3H_5O^-$, *t*-Bu$^-$	0.9	<0.1
		2.2 *sh*[b]	
		5.5	0.1
58	$(CH_3)_2CO^-$	0.0	<0.1
73	*t*-BuO$^-$	2.3	0.1
		4.6	0.3
		6.7 *sh*	
77	Ph$^-$	1.5	2.0
		4.5	0.4
85	$CH_2{=}C(CH_3)COO^-$	0.5	<0.1
89	$(CH_3)_2(OCH_3)CO^-$	1.0	<0.1
		2.2 *sh*	
		5.0 *sh*	<0.1
		6.9	
121	PhCOO$^-$	0.0	88
		0.7	100

[a]m* means metastable ion. [b]*sh* stands for shoulder.

energy in the ET spectrum (see Table 1), whereas maxima occurring above this energy (see Figure 6) should mainly derive from dissociation of core-excited anion states. The m/e = 77 fragment anion is ascribed to formation of the $C_6H_5^-$ species (denoted as Ph$^-$ in Tables 2 and 3). The B3LYP/6-31+G(d) thermodynamic threshold for direct production of Ph$^-$ and its neutral counterpart *t*-BuOOCO$^\bullet$ (where Bu stands for butyl) for cleavage of a C−C bond is about 3.2 eV. A sizably smaller threshold (only about 0.2 eV) is predicted for a simultaneous loss of CO_2 from the latter (see Table 2). Thus, this mechanism must be associated with the most intense (and rather broad) m/e = 77 peak at 1.5 eV, plausibly due to contributions from dissociative channel of both the σ^*_{O-O} and π_3* resonances.

The m/e = 73 anion current, corresponding to the *t*-BuO$^-$ species, also displays a peak at 2.3 eV, which is likely associated with the π_3* resonance. In agreement, the calculations (see Table 2) predict no energy threshold for dissociation of the O−O bond of the molecular anion not only when the negative fragment produced is PhCOO$^-$ (m/e = 121), but even when the negative charge remains on the *t*-BuO moiety (m/e = 73) to give either *t*-BuO$^-$ + PhCOO$^\bullet$ or *t*-BuO$^-$ + Ph$^\bullet$ + CO_2. Moreover, dissociation of the *t*-BuO$^-$ negative fragment into $C_3H_5O^-$ (m/e = 57) and CH_4 is calculated to lead to even more stable products.

The latter decay channel was previously invoked[39] to explain the presence of the m/e = 57 negative current in the DEA spectra of **DTP**. The energies of the m/e = 57 peaks observed here at 0.9 and 2.2 eV are smaller than the thermodynamic threshold (>3.1 eV, see Table 2) calculated for simple cleavage of a C−O single bond to generate a neutral PhCOOO$^\bullet$ radical and a negative m/e = 57 *t*-Bu$^-$ fragment. However, the calculations also predict that loss of CO_2 from the PhCOOO$^\bullet$ neutral radical sizably lowers the energy of the products with the calculated threshold becoming close to zero (see Table 2). Therefore, at variance with **DTP** where the m/e = 57 current below 3 eV must be completely ascribed to the $C_3H_5O^-$

dx.doi.org/10.1021/jp300643e | J. Phys. Chem. A 2012, 116, 3585−3592

species, in **TBPB** some contributions from *t*-Bu^- fragment anions can not be excluded.

The present DEA results also revealed a broad metastable negative ion peak (for a detailed description of metastable peaks, see ref 71 and references therein) with m/e = 49.0 (denoted as m* in Table 3) located at 1.2 eV. Its apparent mass (49.0 = $77^2/121$) is in line with slow (microseconds) consecutive elimination of a CO_2 neutral molecule from the $PhCOO^-$ (m/e = 121) anion to form the Ph^- (m/e = 77) anion. In agreement, the calculated energy threshold (about 0.2 eV) is much smaller than the peak energy.

Although very weak, an m/e = 85 anion current was detected very close to zero energy (Figure 6). The most obvious structure of this fragment would probably be *t*-$BuCO^-$ (C_5H_9O), but according to the calculated energy thresholds, this anion fragment can be formed only at incident electron energies > 2.6 eV (see Table 2). According to the calculations, the occurrence of strong rearrangements to generate one of the (at least) four isomers of the $C_4H_5O_2^-$ negative species (represented in Figure 7 and labeled as 1−4, in order of increasing energy), together with a neutral $PhO^•$ radical and a CH_4 molecule, leads to products sizably more stable (see Table 2) than the neutral ground state of the **TBPB** molecule.

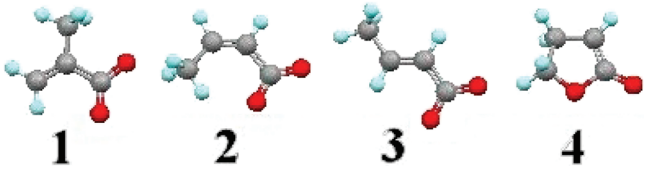

Figure 7. Representation of the B3LYP/6-31+G(d) optimized geometries of the four most stable $C_4H_5O_2^-$ isomers, in order of increasing energy.

A weak m/e = 89 current displayed maxima at energies of 1.0 and 6.9 eV and shoulders at 2.2 and 5.0 eV (Figure 6), the low-energy signals being plausibly associated with dissociation of the π_2* and σ^*_{O-O} and π_3* resonances. The most obvious structure for the m/e = 89 anion fragment seems to be PhC^-, but the calculations predict an energy threshold (6.7 eV, see Table 2) too high except possibly for the 6.9 eV peak. However, an energy threshold < 2 eV is calculated for C(O)−O bond cleavage to give the m/e = 89 *t*-$BuOO^-$ anion fragment, and no threshold at all for a $C_4H_9O_2^-$ isomer (see Table 2) deriving from more complex rearrangements.

A weak m/e = 58 peak was observed at zero energy and is likely due to formation of the acetone anion, following complex rearrangements of the molecular anion. In agreement, the calculations predict the total energy of the $PhCOOCH_3$ and $(CH_3)_2CO^-$ products to be sizably smaller than that of the **TBPB** neutral molecule. Finally, light species with m/e = 15 and m/e = 44, plausibly due to formation of the CH_3^- and CO_2^- anions, respectively, are observed only at incident electron energies above the π_4* anion state; although, according to the calculations, the thermodynamic energy thresholds (1.1 eV and zero, respectively) are by far smaller.

4. CONCLUSIONS

Peroxides represent a strong free-radical source, extensively used as initiators in polymerizations, curing agents in the petrochemical industry, and active components of cosmetics and pharmaceuticals. Their reactivity, however, may also lead to severe disease conditions in humans. Free radical-generating compounds, including in particular *tert*-butyl peroxybenzoate (**TBPB**), have in fact been found to possesses tumor-promoting properties. In the case of peroxides, the mechanism is likely initiated by occurrence of O−O bond cleavage and formation of alkoxyl radicals. The presence of **TBPB** in the intermembrane space of mitochondria in living tissues under reductive conditions would mainly generate benzoate anions and neutral *tert*-butoxy radicals, by far the most abundant species generated by cleavage of the O−O bond of the molecular anion according to the present data. The affinity of the *tert*-butoxy radical (4.524 eV, as calculated here at the B3LYP/6-31+G(d) level) for a hydrogen radical is large enough to abstract a hydrogen atom from ambient lipids,[72] thus initiating the first step of the lipid peroxidation[73] and altering the membrane state, favoring its permeability. It is also to be noticed that, in addition to direct photochemical damage to DNA,[74] the excited molecules produced in skin by solar ultraviolet radiation favor electron transfer to xenobiotic molecules, thus opening DEA channels.

As revealed by the present results, the π-system of **TBPB** plays an important role in the reductive mechanism of radical generation, at least from a quantitative point of view. Because of the presence of a conjugated π-system, its (π*) EA_v is slightly positive, whereas the (σ*) EA_v (−2.0 eV) of the saturated analogue di-*tert*-butyl peroxide is much smaller. Because of the π* nature and low energy of the first anion state of **TBPB**, its electron attachment and DEA cross-sections are much larger. Other conditions being the same, the DEA cross-section increases with the lifetime of the molecular anion with respect to re-emission of the extra electron. In turn, the anion lifetime depends on an inverse fashion on energy. A quantitative evaluation of the total current measured in **TBPB** at zero energy leads to a DEA cross-section about three times as large as that of bromobenzene.[70] Although their yields are 2 orders of magnitude smaller than those of the main products (benzoate anion and *tert*-butoxy neutral radical), the present data reveal that DEA to **TBPB** leads to a variety of other fragments (for instance, the acetone anion) that could induce damages to DNA.

Therefore, within the limits of a gas-phase analysis, the DEA technique can reveal which reactive fragment species can be generated by dissociative electron attachment under conditions of excess negative charge, thus emerging as a useful probe for a preventive prediction of possible damages caused to cellular tissues by reductive processes.

AUTHOR INFORMATION

Corresponding Author

*E-mail: alberto.modelli@unibo.it.

Notes

The authors declare no competing financial interest.

ACKNOWLEDGMENTS

A.M. thanks the Italian Ministero dell'Istruzione, dell'Università e della Ricerca for financial support.

REFERENCES

(1) Duh, Y.-S.; Hui wu, X.; Kaob, C.-S. *Process Saf. Prog.* **2008**, *27*, 89−99.

(2) Buback, M.; Sandmann, J. *Z. Phys. Chem.* **2000**, *214*, 583−607.

(3) Abel, B.; Assmann, J.; Buback, M.; Grimm, C.; Kling, M.; Schmatz, S.; Schroeder, J.; Witte, T. *J. Phys. Chem. A* **2003**, *107*, 9499−9510.
(4) Fujimori, K. In *Organic Peroxides*; Ando, W., Ed.; Wiley: New York, 1992; p 319.
(5) Anbarasan, R.; Babot, O.; Maillard, B. *J. Appl. Polym. Sci.* **2004**, *93*, 75−81.
(6) Barson, C. A.; Bevington, J. C. *J. Polym. Sci., Part A: Polym. Chem.* **1997**, *35*, 2955−2960.
(7) Asandei, A. D.; Saha, G. *J. Polym. Sci., Part A: Polym. Chem.* **2006**, *44*, 1106−1116.
(8) Lai, D. Y.; Woo, Y.; Argus, M. F.; Arcos, J. C. *Environ. Carcinog. Ecotoxicol. Rev.* **1997**, *14*, 63−80.
(9) Tseng, J.-M.; Lin, Y.-F. *Ind. Eng. Chem. Res.* **2011**, *50*, 4783−4787.
(10) Liu, Y.; Fiskum, G.; Schubert, D. *J. Neurochem.* **2002**, *80*, 780−787.
(11) Adam-Vizi, V.; Chinopoulos, C. *Trends Pharmacol. Sci.* **2006**, *7*, 639−645.
(12) Burton, G. J.; Jauniaux, E. *Best Pract. Res., Clin. Obstet. Gynaecol.* **2011**, *25*, 287−299.
(13) Halliwell, B. *Am. J. Med.* **1991**, *91/3*, S14−S22.
(14) Matés, J. M.; Pérez-Gómeza, C.; Núñez De Castro, I. *Clin. Biochem.* **1999**, *32*, 595−603.
(15) Waris, G.; Ahsan, H. *J. Carcinog.* **2006**, *5*, 14−21.
(16) Marnett, L. J. *Carcinogenesis* **1987**, *8*, 1365−1373.
(17) Malins, D. C. *J. Toxicol. Environ. Health* **1993**, *40*, 247−261.
(18) Copeland, E. S. *Cancer Res.* **1983**, *46*, 5631−5637.
(19) DiGiovanni, J. *Pharmacol. Ther.* **1992**, *54*, 63−128.
(20) Bagchi, D.; Bagchi, M.; Stohs, S. J.; Das, D. K.; Ray, S. D.; Kuszynski, C. A.; Joshi, S. S.; Pruess, H. G. *Toxicol.* **2000**, *148*, 187−197.
(21) Greenley, T. L.; Davies, M. J. *Biochim. Biophys. Acta* **1993**, *1157*, 23−31.
(22) Liu, J.; St. Clair, D. K.; Gu, X.; Zhao, Y. *FEBS Lett.* **2008**, *582*, 1319−1324.
(23) Kraus, A. L.; Munro, I. C.; Orr, J. C.; Binder, R. L.; Le Boeuf, R. A.; Williams, G. M. *Regul. Toxicol. Pharmacol.* **1995**, *21*, 87−107.
(24) Hanausek, M.; Walaszek, Z.; Viaje, A.; LaBate, M.; Spears, E.; Farrell, D.; Henrich, R.; Tveit, A.; Walborg, E. F. Jr.; Slaga, T. J. *Carcinogenesis* **2004**, *25*, 431−437.
(25) Saveant, J. M. *Acc. Chem. Res.* **1993**, *26*, 455−461.
(26) Maran, F.; Workentin, M. S. *Electrochem. Soc. Interface* **2002**, *11*, 44−49.
(27) Antonello, S.; Maran, F. *Chem. Soc. Rev.* **2005**, *34*, 418−428.
(28) Kennedy, C. H.; Church, D. F.; Winston, G. W.; Pryor, W. A. *Free Radical Biol. Med.* **1992**, *12*, 381−387.
(29) Antonello, S.; Musumeci, M.; Wayner, D. D. M.; Maran, F. *J. Am. Chem. Soc.* **1997**, *119*, 9541−9549.
(30) Donkers, R. L.; Maran, F.; Wayner, D. D. M.; Workentin, M. S. *J. Am. Chem. Soc.* **1999**, *121*, 7239−7248.
(31) Antonello, S.; Maran, F. *J. Am. Chem. Soc.* **1999**, *121*, 9668−9676.
(32) Baron, R.; Darchen, A.; Hauchard, D. *Electrochim. Acta* **2006**, *51*, 1336−1341.
(33) World Health Organization. *Trans. R. Soc. Trop. Med. Hyg.* **2000**, *94* (Suppl. 1), 36.
(34) Meschnick, S. R.; Taylor, T. E.; Kamchonwongpaisan, S. *Microbiol. Rev.* **1996**, *60*, 301−315.
(35) Sanche, L.; Schulz, G. J. *Phys. Rev. A* **1972**, *5*, 1672−1683.
(36) Schulz, G. J. *Rev. Mod. Phys.* **1973**, *45*, 378−422, 423−486.
(37) Illenberger, E.; Momigny, J. *Gaseous Molecular Ions. An Introduction to Elementary Processes Induced by Ionization*; Steinkopff Verlag Darmstadt, Springer-Verlag: New York, 1992.
(38) Galasso, V.; Kovač, B.; Modelli, A. *Chem. Phys.* **2007**, *335*, 141−154.
(39) Modelli, A.; Galasso, V. *J. Phys. Chem. A* **2007**, *111*, 7787−7792.
(40) Modelli, A.; Jones, D.; Distefano, G. *Chem. Phys. Lett.* **1982**, *86*, 434−437.
(41) Johnston, A. R.; Burrow, P. D. *J. Electron Spectrosc. Relat. Phenom.* **1982**, *25*, 119−133.
(42) Modelli, A.; Foffani, A.; Scagnolari, F.; Jones, D. *Chem. Phys. Lett.* **1989**, *163*, 269−275.
(43) Khvostenko, V. I. *Negative Ion Mass Spectrometry in Organic Chemistry*; Nauka: Moscow, Russia, 1981 (in Russian).
(44) Pshenichnyuk, S. A.; Asfandiarov, N. L. *Eur. J. Mass Spectrosc.* **2004**, *10*, 477−486.
(45) Tseng, J.-M.; Lin, Y.-F. *Ind. Eng. Chem. Res.* **2011**, *50*, 4783−4787.
(46) Frisch, M. J.; Trucks, G. W.; Schlegel, H. B.; Scuseria, G. E.; Robb, M. A.; Cheeseman, J. R.; Scalmani, G.; Barone, V.; Mennucci, B.; Petersson, G. A.; Nakatsuji, H.; Caricato, M.; Li, X.; Hratchian, H. P.; Izmaylov, A. F.; Bloino, J.; Zheng, G.; Sonnenberg, J. L.; Hada, M.; Ehara, M.; Toyota, K.; Fukuda, R.; Hasegawa, J.; Ishida, M.; Nakajima, T.; Honda, Y.; Kitao, O.; Nakai, H.; Vreven, T.; Montgomery, J. A., Jr.; Peralta, J. E.; Ogliaro, F.; Bearpark, M.; Heyd, J. J.; Brothers, E.; Kudin, K. N.; Staroverov, V. N.; Kobayashi, R.; Normand, J.; Raghavachari, K.; Rendell, A.; Burant, J. C.; Iyengar, S. S.; Tomasi, J.; Cossi, M.; Rega, N.; Millam, J. M.; Klene, M.; Knox, J. E.; Cross, J. B.; Bakken, V.; Adamo, C.; Jaramillo, J.; Gomperts, R.; Stratmann, R. E.; Yazyev, O.; Austin, A. J.; Cammi, R.; Pomelli, C.; Ochterski, J. W.; Martin, R. L.; Morokuma, K.; Zakrzewski, V. G.; Voth, G. A.; Salvador, P.; Dannenberg, J. J.; Dapprich, S.; Daniels, A. D.; Farkas, O.; Foresman, J. B.; Ortiz, J. V.; Cioslowski, J.; Fox, D. J. *Gaussian 09*, revision A.02; Gaussian, Inc.: Wallingford, CT, 2009.
(47) Becke, A. D. *J. Chem. Phys.* **1993**, *98*, 5648−5652.
(48) Bair, R. A.; Goddard, W. A. III. *J . Am. Chem. Soc.* **1982**, *104*, 2719−2724.
(49) McMillen, D. F.; Golden, D. M. *Annu. Rev. Phys. Chem.* **1982**, *33*, 493−532.
(50) Reints, W.; Pratt, D. A.; Korth, H.-G.; Mulder, P. *J. Phys. Chem. A* **2000**, *104*, 10713−10720.
(51) Borges do Santos, R. M.; Muralha, V. S. F.; Correia, C. F.; Martinho Simões, J. A. *J. Am. Chem. Soc.* **2001**, *123*, 12670−12674.
(52) DeTuri, V. F.; Ervin, K. M. *J. Phys. Chem. A* **1999**, *103*, 6911−6920.
(53) Koopmans, T. *Physica* **1934**, *1*, 104−113.
(54) Staley, S. W.; Strnad, J. T. *J. Phys. Chem.* **1994**, *98*, 116−121.
(55) Guerra, M. *Chem. Phys. Lett.* **1990**, *167*, 315−319.
(56) Chen, D.; Gallup, G. A. *J. Chem. Phys.* **1990**, *93*, 8893−8901.
(57) Simons, J.; Jordan, K. D. *Chem. Rev.* **1987**, *87*, 535−555.
(58) Hehre, W. J.; Radom, L.; Schleyer, P. v. R.; Pople, J. A. *Ab Initio Molecular Orbital Theory*; Wiley: New York, 1986.
(59) Dunning, T. H., Jr.; Peterson, K. A.; Woon, D. E. Basis Sets: Correlation Consistent Sets. In *The Encyclopedia of Computational Chemistry*; Schleyer, P. v. R., Ed; John Wiley: Chichester, U.K., 1998.
(60) Modelli, A.; Hajgató, B.; Nixon, J. F.; Nyulászi, L. *J. Phys. Chem. A* **2004**, *108*, 7440−7447.
(61) Modelli, A. *Phys. Chem. Chem. Phys.* **2003**, *5*, 2923−2930.
(62) Modelli, A.; Szepes, L. *Chem. Phys.* **2003**, *286*, 165−172.
(63) Burrow, P. D.; Gallup, G. A.; Modelli, A. *J. Phys. Chem. A* **2008**, *112*, 4106−4113.
(64) Pshenichnyuk, S. A.; Asfandiarov, N. L.; Burrow, P. D. *Russ. Chem. Bull., Int. Ed.* **2007**, *56*, 1268−1270.
(65) Modelli, A. *Trends Chem. Phys.* **1997**, *6*, 57−95.
(66) Scheer, A. M.; Burrow, P. D. *J. Phys. Chem. B* **2006**, *110*, 17751−17756.
(67) Modelli, A.; Burrow, P. D. *J. Phys. Chem.* **1984**, *88*, 3550−3554.
(68) O'Malley, T. F. *Phys. Rev.* **1966**, *150*, 14−29.
(69) Guerra, M.; Jones, D.; Distefano, G.; Scagnolari, F.; Modelli, A. *J. Chem. Phys.* **1991**, *94*, 484−490.
(70) Modelli, A. *J. Phys. Chem. A* **2005**, *109*, 6193−6199.
(71) Pshenichnyuk, S. A.; Modelli, A. *Int. J. Mass Spec.* **2010**, *294*, 93−102.
(72) Gregory, N. L. *Nature* **1966**, *212*, 1460−1461.
(73) Niki, E.; Yoshida, Y.; Saito, Y.; Noguchi, N. *Biochem. Biophys. Res. Commun.* **2005**, *338*, 668−676.

(74) Mukhtar, H.; Elmets, C. A. *Photochem. Photobiol.* **1996**, *63*, 356−357.